Corrugated Rollable Tubular Booms

Juan M. Fernandez*
NASA Langley Research Center, Hampton, VA 23681, USA

and

Christopher E. Volle†
Old Dominion University, Norfolk, VA 23529, USA

A promising candidate for a new class of deployable composite boom is the COrrugated ROllable TUbular Boom (COROTUB), which is to be employed on future large space structures by the National Aeronautics and Space Administration (NASA). This is due to its two corrugated thin-shells forming a closed-section, which yields high bending and torsion stiffness, allowing for high dimensional stability. The corrugation geometry that dictates the boom cross-section shape is completely defined by closed-form analytical equations given a set of key input parameters available to the designer. Parametric studies changing two geometric variables are used to evaluate which parameters most influence the cross-section's area moment of inertia and torsional constant. The number of corrugations, flattened height of the boom, and concave and convex corrugation radii are varied to study the complete boom design space. Deeper corrugations increase the local buckling loads (crimpling) of the thin-shell boom but reduce the area moment of inertia and therefore the global Euler buckling load of the compressive member, and thus a fine balance is sought. Finite element analyses of pure bending and compression load cases for 1.22 m boom specimens were carried out to study this design trade-off in detail. Based on previous work, several thin-ply composite laminates have been selected for the different shells that form the cross-section. Feasible boom designs with a maximized stiffness and load-carrying capacity will be manufactured to study their rollability and for experimental characterization. Structural characterization tests and additional numerical analyses will provide guidelines towards future corrugated boom designs and adequate boundary conditions to maximize the boom bending strength.

Nomenclature

h = flattened boom height
n = number of corrugations
w = web length
r_w = web radius
α_w = subtended angle of web segment, created by ∠**ABC**
r_v = radius of convex shell segment
r_c = radius of concave shell segment
α_v = subtended angle of convex shell segment
α_c = subtended angle of concave shell segment
r_{sh} = radius of generic shell segment
R_o = radius of circle used for construction of the geometry, the concave segment centers lie on this circle
R_i = radius of circle used for construction of the geometry, the convex segment centers lie on this circle
R_w = distance from the origin to the center of the web radius arc, point **B**
t_{sh} = thickness of generic shell segment

* Research Aerospace Engineer, Structural Dynamics Branch, NASA LaRC, 4 West Taylor Street, Mail Stop 230. AIAA Member.
† Master's Student Candidate, Department of Aerospace Engineering, Old Dominion University, 5115 Hampton Blvd, Norfolk, VA 23529. AIAA Student Member.

γ = angle between vertical axis and center of web radius arc, created by ∠**AOB**
β = angle between the center of web segment arc and center of corrugation segment arc **C**, created by ∠**BOC**
ϕ = angle between any remaining convex and concave radius, here made by ∠**COD** and ∠**DOE**
ϵ = angle created by ∠**OBC**
λ_i = angle created between the horizontal line stemming from a corrugation arc center and a line connecting the centers of two curved segments.

I. Introduction

Deployable composite booms are particularly attractive to the small satellite community given their high packaging volume efficiency that enables relatively large spacecraft systems required for power generation, communications or propulsion to be housed within the small confines of these platforms[1]. Increasing the size of these deployable systems greatly affects the capabilities of small satellites from a scientific and exploration perspective, even enabling them to travel further from Earth[2]. In general, industry has been focusing on further developing rollable boom concepts that use open cross-sections, like the family of Storable Tubular Extensible Member (STEM) and its variations[3] and the Triangular Rollable And Collapsible (TRAC) boom[4], whose ease of manufacturing reduces overall part cost, particularly at larger scales. The high volume demands for some of the current and proposed large constellations of small satellites have only exacerbated the tendency to move towards simplistic designs, and even automated fabrication production.

Over the years, there have been several developments to try to improve the biggest disadvantage of open-section boom structures, which is their low torsional stiffness that can cause premature buckling and low deployed accuracy and stability and limit their scalability. These range from partially or fully closing the cross-section using: discrete lacing elements[5]; continuously bonded or stitched inner shells[6]; interlocking teeth[7]; elastic hinges[8]; outer plastic[1,9] or braided sleeves[10,11]; friction[12]; or mechanically or magnetically latching the two free edges of slit tubes[13]; However, most of these designs yield a final product that either packages much less efficiently than anticipated or has a lower torsional stiffness than a true closed-section part of single construction. Also, the asymmetric nature of some of these designs reduces their load carrying capability when subjected to eccentric or asymmetric loads. To date, the only monolithic closed-section tubular thin-shell structure is the Collapsible Tubular Mast (CTM)[1-2,14-17]. The CTM geometry consists of two thin-shell omega-shaped halves formed by three curved segments that are bonded at a flat region called the web.

The NASA Langley Research Center (LaRC), as part of the Deployable Composite Booms (DCB) project[18], has been developing recently a family of composite CTM booms that scale the size range needed for NASA's near-term small satellite applications, including solar sails. The target range is 5-20 m long booms able to package on CubeSats and larger platforms[2]. This includes, generating for the first time, bistable monolithic closed-section rollable structures, in this case of the CTM geometry[19]. Both symmetric (more common boom form) and asymmetric (more favorable towards producing bistability) CTM designs and analytically predictive models have been developed[20]. Another project goal was to simplify the manufacturing process for the various scales and develop out-of-autoclave processes compatible with the long slender nature of these composite elements[21]. Figure 1 (b) shows the new dedicated large equipment built to fabricate long booms, including the low coefficient of thermal expansion (CTE) carbon foam molds, tunnel composite curing convection oven, rolling cart and other associated hardware for rotating, lifting, coupling and separating the boom molds. In the picture a 16.55 m CTM boom is being held horizontally by three people.

(a) (b)

Fig. 1. (a) A CTM (left) and the new COROTUB (right) of the same size, i.e. boom flattened height, $h = 130$ mm; (b) Large-scale boom fabrication facility at LaRC capable of producing booms up to 17 m long in the tunnel composite curing oven.

This paper presents a new monolithic closed-section boom concept, the Corrugated Rollable Tubular Boom (COROTUB). Figure 1 shows a CTM and a COROTUB side by side. The latter structure has a corrugated thin-shell wall that also ends in two flat regions used to bond the two boom halves. The boom is flattened by pulling these two webs apart and then rolls on a cylindrical spool. Work from the Tokyo Institute of Technology on a corrugated closed-section boom concept targeting much smaller cross-sections with a small number of corrugations has also been publically presented in recent years[22]. One-meter booms with two corrugations were recently manufactured, initially characterized and functionally tested using a deployment mechanism by this group, though only the softer laminate designs, which are prone to creep, were able to roll without damage[23].

The full design space of corrugated closed-section booms is being evaluated at LaRC to yield the best compromise between rollability, boom specific stiffness and strength on large scale designs. While the structural benefits offered by the corrugations at relatively small boom sizes (h < 150 mm) is limited by the shallowness of the corrugations required to roll the booms without damage. These unique geometric features enable much stiffer and stronger booms for large scale designs. The improvements may allow monolithic beam-column structures to compete with truss alternatives at a longer boom regime.

Traditionally, multiple-shell boom designs (two or more shells affixed) like the TRAC, CTM or COROTUB cannot increase their shell thickness at larger sizes without an impact to packaging efficiency. As the boom grows in size, the designs are more prone to local buckling because of the low thickness-to-radius ratio (t_{sh}/r_{sh}) of the shell segments that form the cross-section. This poses a real technology scalability limitation. It is such a limitation that the corrugated designs are trying to restrict. By decreasing the shell radii r_{sh} to those used on much smaller traditional boom designs, the local buckling stresses of the various shell segments, i.e. those that cause section crimpling or local snap-through, are increased significantly. This principle is already exploited in other types of thin-shell compression members, like large cylindrical shell structures used on aircraft and launch vehicles. It is common knowledge that implementing a corrugated shell design can greatly increase the axial compressive load capability of such elements[24]. It has also been demonstrated that shell corrugations can make these structures insensitive to fabrication or loading imperfections[25]. However, there are additional intrinsic benefits to ultra-thin-shell slender rollable composites structures. The expected benefits of COROTUBs over CTMs for scalability due to the thin-wall shell corrugation (r_{sh} decreases while t_{sh} remains similar as cross-section scales up) are:

- Increased resistance to local buckling allows higher bending moments at the root of the boom. This can also increase the load carrying capability of the boom while it is being deployed and the root cross-sectional area is still partially developed.
- Reduced boom transition length from flat to deployed, which enables more compact deployment mechanisms and allows larger inertias exiting the deployer with the resultant increased load bearing capacity.
- Reduced boom shape deformation during prolonged stowage in a rolled configuration, i.e. loss of dimensional stability after stowage. This has benefits in strain-energy driven deployment concepts and against flattening of the cross-section with the resultant decrease of load bearing capability and pointing accuracy.
- Reduced global manufacturing shape distortion, i.e. loss of dimensional stability during fabrication, due to the increased structural depth of the thin shells provided by the corrugations that reduce cure-induced deformations and residual stresses.

II. Analytical Model

An analytical model was created to fully define the cross-section of COROTUB designs from a series of geometrical input parameters. When the number of corrugations n, flattened boom height h, and web length w are set, it is possible to determine the complete cross-sectional geometry by selecting the radii of the corrugations, though an additional condition for the positioning of the web radius r_w is required. These parameters are illustrated in Fig. 1. The corrugation radii are divided into two types: concave r_c and convex r_v. The convex radius r_v and concave radius r_c lie on the circles created by R_i and R_o, respectively. All corrugation arcs are tangent to one another to create a smooth transition between the corrugations. The web radius r_w is tangent to the web and the first corrugation convex radius.

In this paper, the geometric parameters h, n, w, r_w, r_c, and r_v are pre-defined. Also one of these three conditions for the center of the arc created by r_w at point **B** needs to be selected: the value of its subtended angle α_w, the web radius arc is tangent to either the inner or outer radius R_i or R_o, or the center of the web radius arc lies on R_o. In the geometry presented in Fig. 2, the center point of the web radius arc lies on R_o at the point **B**. Undefined parameters can be determined as a relation between some other parameters, reducing the number of unknowns in the system. A piece-wise determination of the geometry of the cross-section, i.e. step-by-step determination of the equations in the

analytical model, starts with finding γ using ΔOAB. Then, ϵ is found using the law of cosines on $\Delta \boldsymbol{OBC}$. Given the condition where the web radius r_w lies on the outer geometric circle R_o, R_w will be equal to R_o. The particular web radius r_w in Fig. 2 is depicted as equal to the corrugation concave radius r_c, though this is not a necessary condition and the equations allow for different radii. The angles γ and ϵ can then be combined in Eq. 3 and 7. Law of cosines is also used to find ϕ. Equations 1 to 6 are then plugged into Eq. 7 and Eq. 9, leaving a system of two equations with two unknown variables, R_i and R_o, to be solved numerically. There is no single design criteria which can be tied to R_i and R_o. A maximum horizontal boom width is not the same as $2R_o$ unless $r_v < R_o - R_i$, so it is not used as criteria.

There is a special geometric case when R_i is equal to R_o that reduces the equations and leaves one geometric radius to solve for directly. This new $R = R_i = R_o$ allows the equations to be rearranged allowing to solve the equations for any chosen parameter. This cannot be done when these radii are different because the restrictions on possible values of R_i and R_o are too difficult to predict due to the complexity of the equations. There is another special case where corrugation radii are equal, which makes the r_c and r_v tangent to the geometric radii R_i and R_o, respectively. This creates the relation $r_v = r_c = r_{corrug} = R_o - R_i$.

The angles λ_i, which define the start and end angles of the arcs and used for plotting the geometry, are derived from the solved geometry. For example, the total subtended angle of the first concave corrugation (the one closest to the boom web) is the sum of $\lambda_1 (= \alpha_w) + \lambda_2$, and that of first convex corrugation (not counting the web-adjacent convex correction) is $\lambda_2 + \lambda_3$. These two make up the alpha, which is the subtended angle, or span of the corrugation. The general form of this is $\alpha_i = \lambda_i + \lambda_{i+1}$. To clarify, λ_i is used for plotting the geometry, rather than solving the geometry.

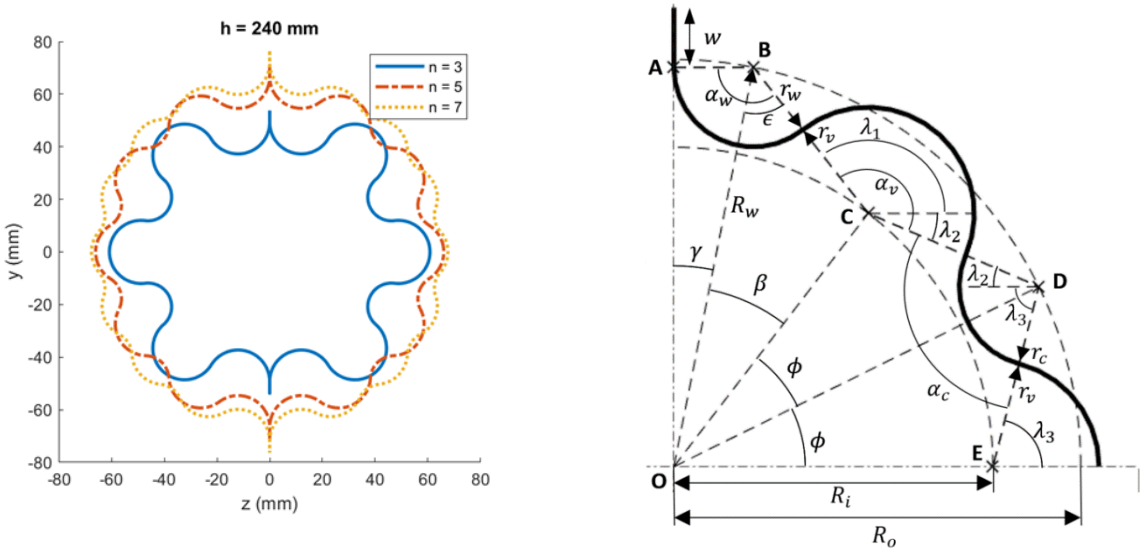

(a) (b)

Fig. 2. (a) Several COROTUB cross-sections with 3, 5, and 7 corrugations for the same boom flattened height of $h = 240$ mm. All dimensions of geometric parameters are in milimeters. The additional constant parameters used are $w = 9$, $r_w = 12$, $r_v = 12$, $r_c = 9$; (b) One quarter of the double-symmetrical COROTUB cross-section for a 3 corrugation version showing all the geometric parameters used to define the complex shape.

$$\gamma = \operatorname{asin}\left(\frac{r_w}{R_w}\right) \tag{1}$$

$$\epsilon = \operatorname{acos}\left(\frac{R_i^2 - (r_w + r_v)^2 - R_w^2}{-2(r_w + r_v)R_w}\right) \tag{2}$$

$$\alpha_w = \frac{\pi}{2} - \gamma + \epsilon \tag{3}$$

$$\beta = \operatorname{acos}\left(\frac{(r_w + r_v)^2 - R_w - R_i^2}{-2R_w R_i}\right) \tag{4}$$

$$\phi = \operatorname{acos}\left(\frac{(r_v + r_c)^2 - R_i^2 - R_o^2}{-2R_iR_o}\right) \tag{5}$$

$$\alpha_c = 2\operatorname{asin}\left(\frac{R_i}{r_v + r_c} sin\phi\right) = \lambda_2 + \lambda_3, \qquad \alpha_v = \alpha_c + \phi = \lambda_1 + \lambda_2 \tag{6 a, b}$$

$$\frac{\pi}{2} = \gamma + \beta + \phi(n-1) \tag{7}$$

$$h = 2[w + (r_w + r_v)\alpha_w + (r_v + r_c)(\alpha_1 + \alpha_2)] \quad when\ n = 3 \tag{8}$$

or, in general,

$$h = 2\left[w + (r_w + r_v)\alpha_w + (r_v + r_c)\sum_{k=1}^{n-1}\alpha_k\right] \tag{9}$$

III. Parametric Analysis

A. Materials

With the analytical model derived for the COROTUB, a series of parametric studies can be conducted to evaluate how geometric, material, and layup designs influence stiffness properties, as well as other design metrics like coiled diameter or bistability. In this first study the effects of material and layup design were not studied in an effort to decouple the geometric and laminate designs, and thus only the geometric parameters were varied. Optimal cross-sections can ultimately be obtained by maximizing the area moments of inertia and torsional constants while satisfying a set of system requirements (volume, mass, bistability, etc.). Table 1 shows the material forms and mechanical properties of the thin-ply composites and adhesive used for the parametric analysis.

Table 1. Material properties of thin-ply composites and adhesive

Label	Material Form	Fiber/Resin	E_1 (GPa)	E_2 (GPa)	ν_{12}	G_{12} (GPa)	Thickness t (μm)
$_C$	Unidirectional (UD)	MR60H/PMT-F7	174.4	8.4	0.259	6.4	42.0
PW_C	Plain Weave (PW)	M30S/PMT-F7	94.2	94.2	0.026	3.9	62.5
$_A$	Adhesive Film	Hysol EA9696	2.1	2.1	0.300	0.6	100.0

This materials are combined to form composite laminates that have been previously used at LaRC with good success to fabricate CTM and other types of high-strain composite rollable booms[1,19]. This first study focuses on double-symmetrical corrugated boom designs both from a geometric and layup perspective and thus detailing one quarter of the cross-section like in Fig. 2 b) defines the entire boom. Table 2 shows the laminate properties used in the different shell segments of the booms analyzed in the parametric studies. For every design, ply drops are incorporated between the convex and concave segments and web radius to reduce the boom coiled strain energy and material strain levels because in most parametric studies $r_v \geq r_c$ or r_w.

Table 2. Laminate properties used in the different shell sections of the booms analyzed in the parametric studies.

Shell section/segment	Radius	Laminate	E_1 (GPa)	E_2 (GPa)	ν_{12}	G_{12} (GPa)	t_{sh} (μm)
Convex	r_v	$[45PW_C/0_C/45PW_C]$	55.5	27.5	0.819	36.0	167.0
Concave and Web radius	r_c and r_w	$[45PW_C/0_C]$	79.9	15.7	0.819	19.7	104.5
Web (flat)	N/A	$[45PW_C/0_C/0_A/0_C/45PW_C]$	54.7	18.8	0.776	20.5	309.0

B. Area Moments of Inertia and Torsional Constant

Determining the boom area moments of inertia about the principal axes, I_{yy} and I_{zz}, and torsional constant, J, is critical for fulfilling system requirements for bending and torsional stiffnesses. Optimal cross sectional geometries of the boom that maximize these metrics, and therefore the stiffnesses, are obtained through parametric analysis. The effective elastic and shear modulus of the boom are dependent on the material properties and are not part of the geometric optimization. In the extended configuration, the booms are oriented as shown in Fig. 2. The geometric

centers of the cross sections are placed at the origin of the $y-z$ coordinate system. Based on relevant geometric parameters such as the radii and lengths of circular arcs, flattened height, web length, and subtended angles, the boom's cross section is discretized into the (y,z) coordinates. Thus, each segment consisting of a pair of (y,z) coordinates is then idealized as a rectangle rotated about the origin by θ. The area moments of inertia of every segment about their own centroid relative to the y and z axes, I_{y_j} and I_{z_j}, are found with the following equations. Let any given rectangular segment be denoted with the subscript $j = 1, \dots, m$, where m is the total number of segments. l_j and t_j are the length and thickness of each segment.

$$I_{y_j} = \frac{1}{12} l_j t_j (l_j^2 \sin^2\theta + t_j^2 \cos^2\theta) \tag{19}$$

$$I_{z_j} = \frac{1}{12} l_j t_j (l_j^2 \cos^2\theta + t_j^2 \sin^2\theta) \tag{20}$$

The corrugated boom's area moments of inertia can be found by summing I_{y_j} or I_{z_j} through the parallel axis theorem, as shown below. A_j is the area of each segment and d_j is the distance from each segment's centroid to the y or z axis.

$$I_{yy,zz} = \sum_{j=1}^{m} I_{y,z_j} + A_j {d_j}^2 \tag{21}$$

The torsional constant is found by summing the torsional constants of the web as open sections, J_O, and the circular segments as the closed sections, J_C, as shown below. A_E is the total enclosed area in the closed section.

$$J_O = \sum_{j=1}^{m} \frac{1}{3} l_j {t_j}^3 \tag{22}$$

$$J_C = 4{A_E}^2 / \sum_{j=1}^{m} \frac{l_j}{t_j} \tag{23}$$

C. Parametric Studies

Due to the complex cross-section of the boom, the effects of many geometric parameters on the various measures of boom stiffness must be evaluated. The approach followed was to study the variation of two geometric parameters at a time while fixing the rest to assess trends that could lead to future design criteria for these types of boom structures. For all these analyses, the geometric condition that the center point of the web radius arc lies on R_o at the point **B** was assumed, which is in line with the designs from Fig. 2.

A parametric study of the boom flattened height h and the number of corrugations n has found that the inertias and torsional constant grow as these parameters increase. A set of cross-sections with constant h and varying n is shown in Fig. 2(a). Results of the analysis are shown in Fig. 3. The fixed input geometric parameters were: w = 9 mm, r_w = 12 mm, r_v = 12 mm, and r_c = 9 mm. No current NASA applications anticipate needing a boom size of a flattened height larger than 400 mm. As expected, the flattened height, which determines the overall boom size, has a predominant effect on the inertias for any given number of corrugations. For a fixed flattened height (boom size), increasing the number of corrugations makes the corrugations shallower and thus increases the inertia. For a very large number of corrugations and large convex radius the results approach an uncorrugated Collapsible Tubular Mast (CTM), the limiting case of a boom with an infinite number of corrugations. Inertia also grows faster with increasing corrugation numbers at a higher value of h than at a lower value. In other words, a high number of corrugations provides a larger benefit to inertia when h is large. These observations are true for all calculated inertias, I_{yy}, I_{zz}, and J.

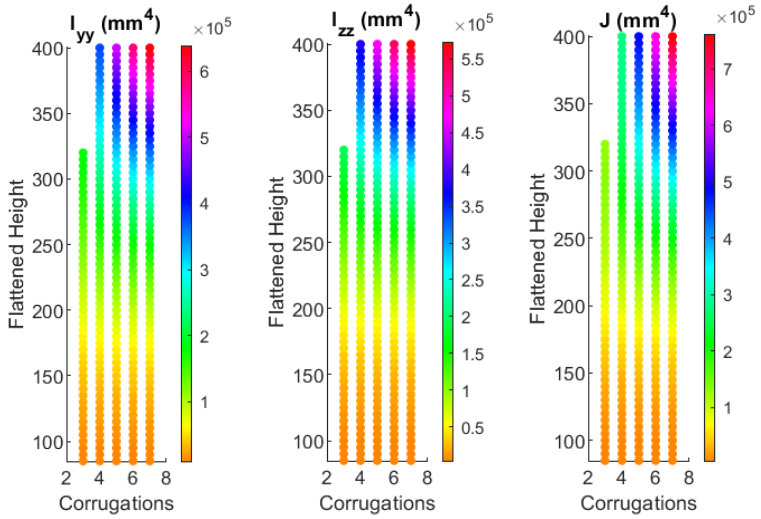

Fig. 3. Parametric study between flattened height h (90 - 400 mm) and number of corrugations n (3 - 7) for w = 9 mm, r_w = 12 mm, r_v = 12 mm, and r_c = 9 mm.

The next parametric study evaluated the number of corrugations n and the corrugation radius r_{corrug} assuming the special case where this radius is the same in the convex and concave shell segments, i.e. $r_{corrug} = r_v = r_c$. The fixed input geometric parameters were: h = 240 mm, w = 9 mm, and r_w = 12 mm. Similar to the previous parametric study, inertias increase with the number of corrugations n, as well as overall corrugation radius r_{corrug}. This is shown in Fig. 4. As r_{corrug} increases, the corrugations in the boom cross-section become shallower, increasing the amount of material further from the centroid of the boom and the total area enclosed. When the corrugation radius continues to increase, the corrugations almost disappear entirely, reducing the cross-section to the shape of the CTM boom. For a certain r_{corrug}, increasing the number of corrugations causes these to become shallower as well. Eventually the system of equations is unable to maintain the parameters and conditions set while solving the missing geometric values. This results in the missing points in the top right corner of the plots in Fig. 4. This holds true for all parametric studies presented in this paper. Inertias grow faster with increasing corrugation numbers at a lower value of r_{corrug} than at a higher value. In other words, a high number of corrugations provides a larger benefit to inertia when r_{corrug} is small. The design criteria for these booms was partially dictated by the material used for manufacturing. A minimum corrugation radius of 9 mm selected for all curvatures was due to the minimum allowable bending radius of curvature to prevent laminate damage and/or plastic deformation. At this boom size, there is currently no interest in exploring designs using corrugation radii higher than 25 mm, or more than 7 corrugations.

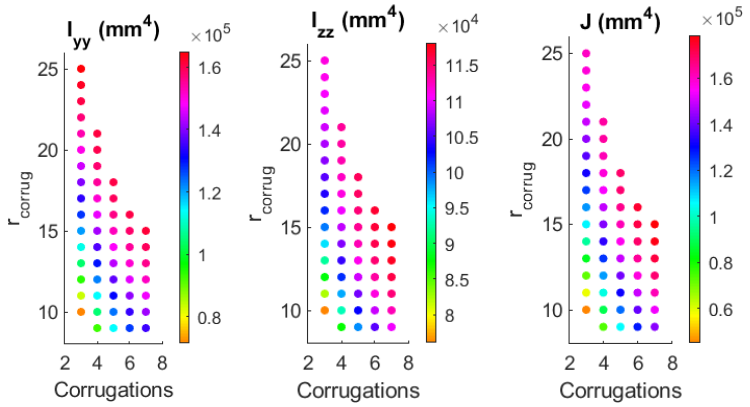

Fig. 4. Parametric study between corrugation radius r_{corrug} (9 – 25 mm) and number of corrugations n (3 – 7) for h = 240 mm, w = 9 mm, r_w = 12 mm. Here, $r_{corrug} = r_c = r_v$.

Similar to the previous studies, inertias increase with increasing convex corrugation radius r_v and number of corrugations n. This is shown in Fig. 5. The fixed input geometric parameters were: h = 240 mm, w = 9 mm, r_w = 12 mm and r_c = 12 mm. As r_v increases, the convex corrugations become more bulbous, stretching away from the center of the geometry and increasing the inertia in all axes. The values of area moment of inertia and the torsional constant increase at a higher rate by increasing number of corrugations n at a lower r_v value than at a higher r_v. Also, the inertias grow more rapidly with r_v. Inertia also grows faster with increasing corrugation numbers at a higher value of h than at a lower value. In other words, a high number of corrugations provides a larger benefit to inertia when h is large. Inertias grow faster with increasing corrugation numbers at a higher value of r_{corrug} than at a lower value. In other words, a high number of corrugations provides a larger benefit to inertia when r_{corrug} is large

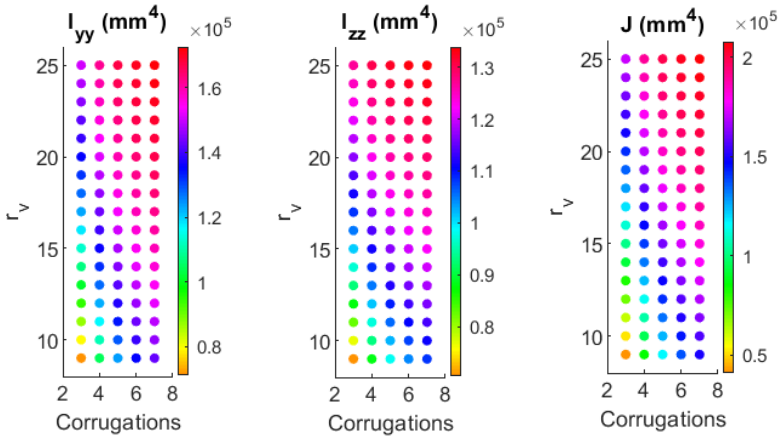

Fig. 5. Parametric study between convex corrugation radius r_v (9 – 25 mm) and number of corrugations n (3 – 7) for h = 240 mm, w = 9 mm, r_w = 12 mm and r_c = 12 mm.

Unlike the previous parametric studies, a comparison of concave corrugation radius r_c and number of corrugations n is more complicated. The fixed input geometric parameters were: h = 240 mm, w = 9 mm, r_w = 12 mm and r_v = 12 mm. As shown in Fig. 6, all inertias grow with increasing n. I_{yy} increases overall, but for $n = 4$, it peaks near r_c = 20 mm (80% of the maximum r_c evaluated of 25 mm). I_{zz} increases with decreasing r_c as the cross-section becomes taller. J increases with increasing r_c only for $n = 3$. For $n = 4$ to 7, as r_c increases, the J values reach a peak about half-way through the range of r_c values assessed. Overall, the data suggests a low-to-medium-range r_c is required to maximize I_{yy}, I_{yy}, and J, under this set of input parameters.

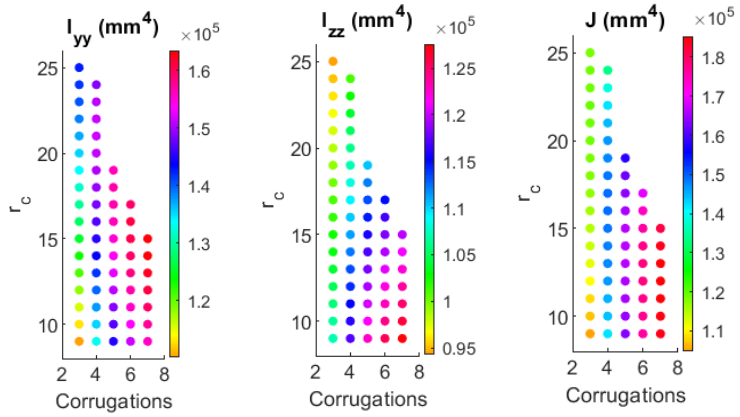

Fig. 6. Parametric study between concave corrugation radius r_c (9 – 25 mm) and number of corrugations n (3 – 7) for h = 240 mm, w = 9 mm, r_w = 12 mm and r_v = 12 mm.

In a parametric study between the convex corrugation r_v and concave corrugation r_c, the trends in variations of inertias between designs with different number of corrugations n (3 to 5) are similar as shown in Fig. 7. The fixed input geometric parameters were: h = 240 mm, w = 9 mm, and r_w = 12 mm. For all n values evaluated, the inertia

and torsional constant increases with increasing r_c. I_{yy} increases with both r_v and r_c for all n, but r_c has a greater effect than r_v. Under closer inspection and for a given r_v and r_c, I_{yy} increases with increasing n. In other words, picking a I_{yy} point from the $n = 3$ graph ($r_v = 10, r_c = 25$, so $I_{yy} \cong 1.46 \cdot 10^5 \text{mm}^4$) and comparing this value to the same point on either $n = 4$ or $n = 5$ shows a higher value of I_{yy}. This is consistent with observations in the previous parametric studies presented.

For all corrugation numbers I_{zz} increases with increasing r_c but decreases with increasing r_v. As the r_c gets larger or the r_v gets smaller, less material is located towards the center of the boom, the corrugations become more shallow, and the I_{zz} increases. r_c has a much larger effect on the rotational inertia J than r_v as the area inside the cross-section for a given fixed size (h value) is heavily influenced by the radius of the convex segments r_c. J is greatest when r_v is in the middle of the tested range as r_c increases.

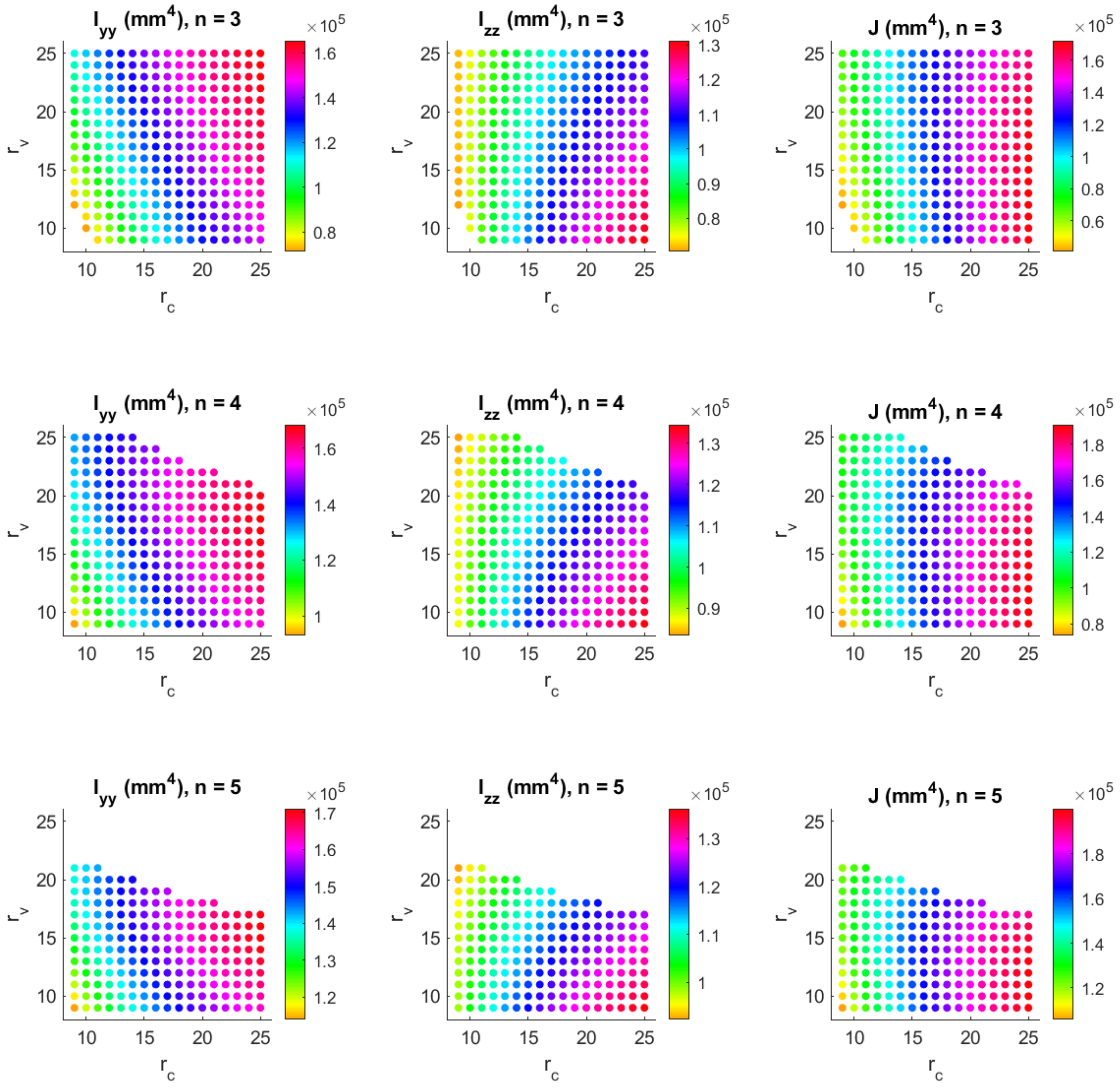

Fig. 7. Parametric study between convex corrugation radius r_v (9 – 25 mm) and concave corrugation radius r_c (9 – 25 mm) for several number of corrugations n (3 – 5) and for h = 240 mm, w = 9 mm, r_w = 12 mm.

In the parametric study where the corrugation radius r_{corrug} is compared to the web radius r_w, inertias increase for all values of increasing r_{corrug}, as shown in Fig. 8. This is the special case assuming this radius is the same in the convex and concave shell segments, i.e. $r_{corrug} = r_v = r_c$. The fixed input geometric parameters were: h = 240 mm and w = 9 mm. In general, all inertias increase with decreasing r_w at high values of r_{corrug}, but comes almost

insignificant at low values of r_{corrug} and low corrugation numbers n. The trends for I_{yy} and J are similar for all number of corrugations, but I_{zz} peaks at high values r_{corrug} and low values of r_w for low number of corrugations ($n \leq 3$), and drift towards the middle range of the r_{corrug} as n increases. It is thus preferred to have the smallest web radius r_w allowed by the composite laminate.

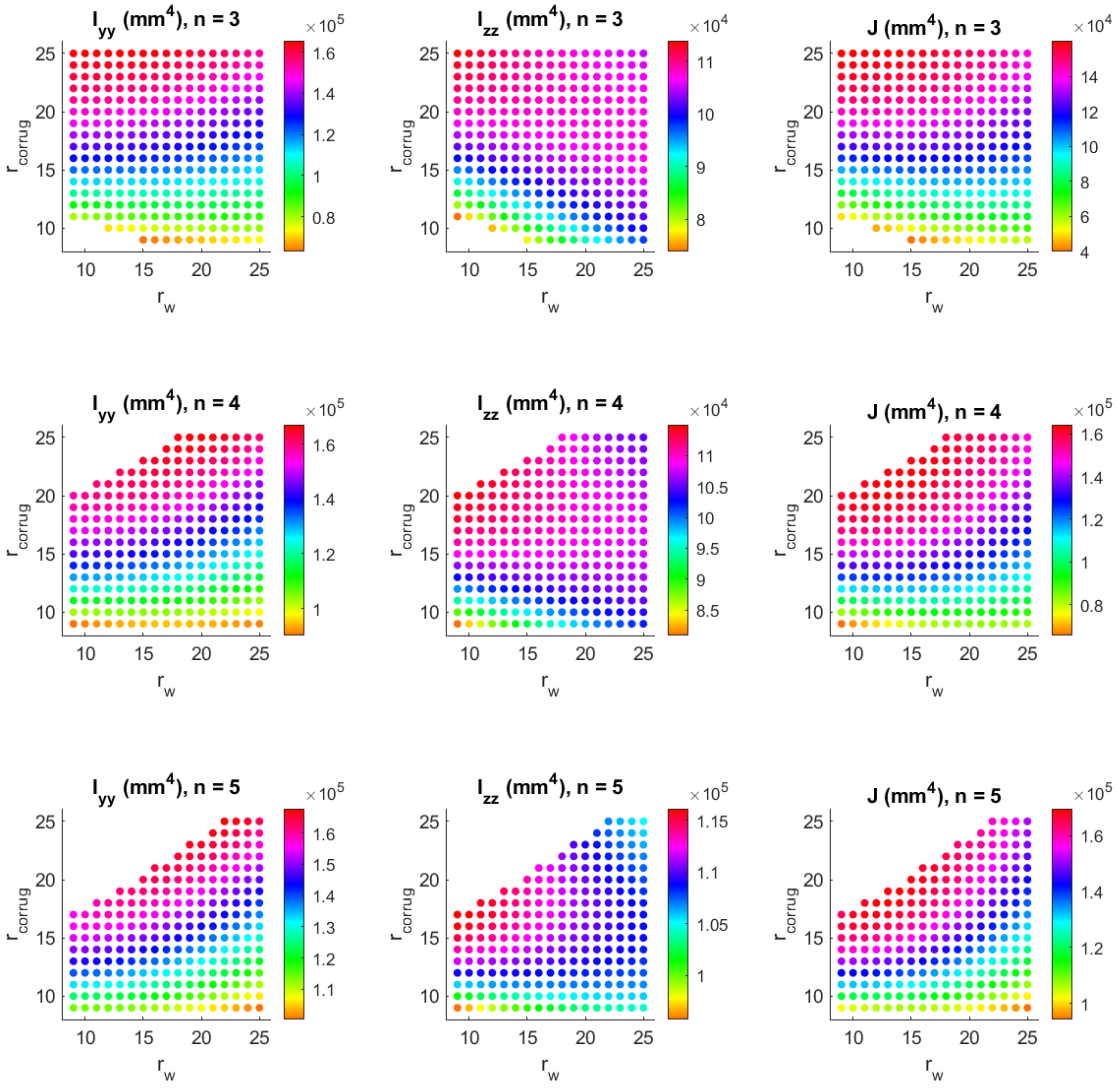

Fig. 8. Parametric study between corrugation radius r_{corrug} (9 – 25 mm) and web radius r_w (9 – 25 mm) for several number of corrugations n (3 – 5) and for h = 240 mm and w = 9 mm. Here, $r_{corrug} = r_c = r_v$.

IV. Structural Analysis

This section will describe the effects of the area moment of inertia and torsional stiffness on the bending and compressive strengths of the corrugated booms. Three geometries of the same flattened height h will be explored. The number of corrugations n is the varying geometric parameter, while the remaining parameters remain constant. These were: h = 240 mm, w = 9 mm, r_w = 12 mm, r_v = 12 mm, and r_c = 9 mm. Figure 9 shows the I_{yy}, I_{zz} and J for n = 3, 4 and 5. For increasing number of corrugations n, all the inertias increase, particularly the rotational inertia.

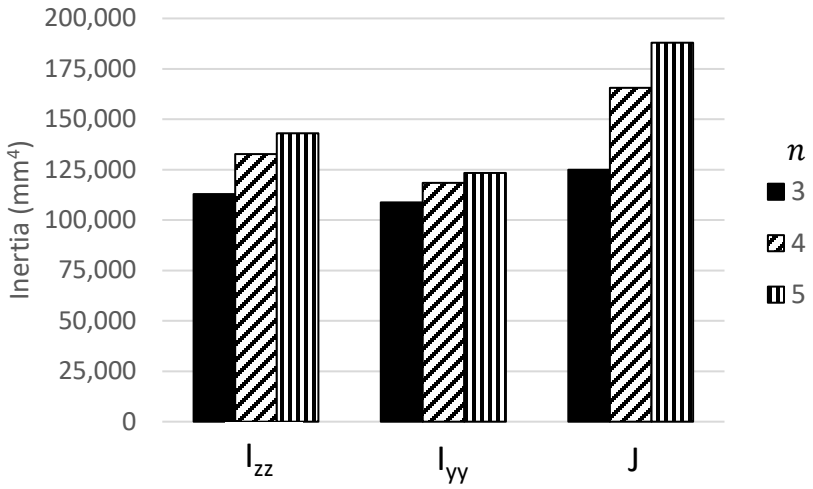

Fig. 9. Area moment of inertia in the *y* and z axis, I_{yy} and I_{zz}, and torsional constant *J* for several number of corrugations $n = 3$, 4, and 5.

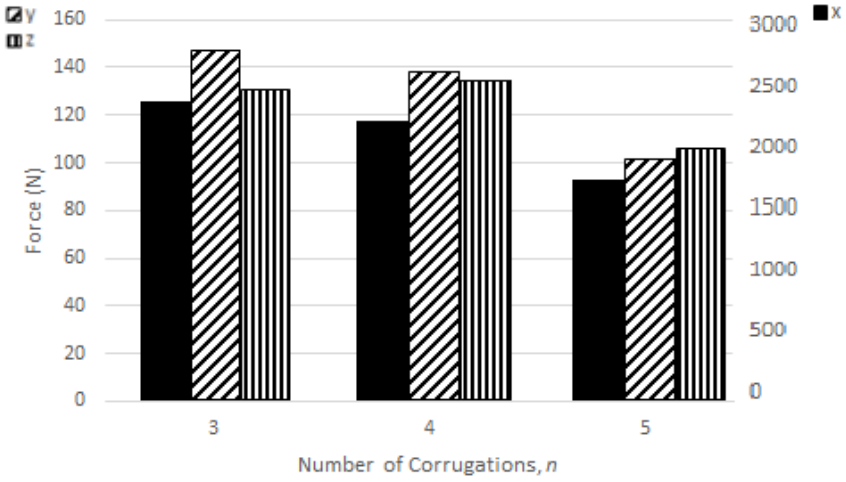

Fig. 10. Critical loads in pure bending (y and z) and compression (x) for several number of corrugations n = 3, 4, and 5.

Short 1.22-m-long boom structural models of the three geometries described in this section were created in Abaqus. The objective was to perform a buckling analysis to identify the critical loads for different load cases as well as the buckling modes for boom designs with a different number of corrugations. The booms were arranged under fixed-free cantilever boundary conditions. All the end nodes corresponding to the fixed end, i.e. boom root, were tied to a control node in the centroid of the cross-section, where all degrees of freedom (translational and rotational) were set to zero. All the end nodes corresponding to the free end, i.e. boom tip, were tied to a control node in the centroid of the cross-section, where uniaxial loads were applied. Bending simulations, with an applied side tip load in the *y* and *z* axis, were performed. The compression simulations applied an axial tip load in the -*x* direction, with an additional side load in the *z* axis of 1% of the previously found bending load failure in order to break symmetry of the boom and allow a buckled solution to be found, i.e. surpass the load bifurcation phenomenon. Loads were applied in a monotonically-increasing fashion using a nonlinear geometric static load analysis step. Figure 10 presents the maximum uniaxial loads in the -*x*, +*y* and +*z* directions achieved before the analysis time increments became extremely small, which translated to the initiation of local buckles. At that moment the analysis was stopped and renderings of the buckled shaped were taken. Figure 11 presents the buckled boom deformed shapes at the end of the bending and compression loading steps.

Several conclusions can be drawn from the computational finite element model results. Even though the inertias get larger with the number of corrugations, as shown in Fig. 9, the maximum compression load F_x is reached at a specific number of corrugations (in this case $n = 4$). A higher number of corrugations produces shallower corrugations, which develop early buckling in the thinner concave shell sections (Fig. 11(c)), while booms with fewer and deeper

corrugations fail at the web or web-adjacent radius (Fig. 11(a) and (b)). Therefore, the first conclusion is that corrugations become less efficient as you increase their number beyond a certain number. A finite element analysis study can determine that value efficiently.

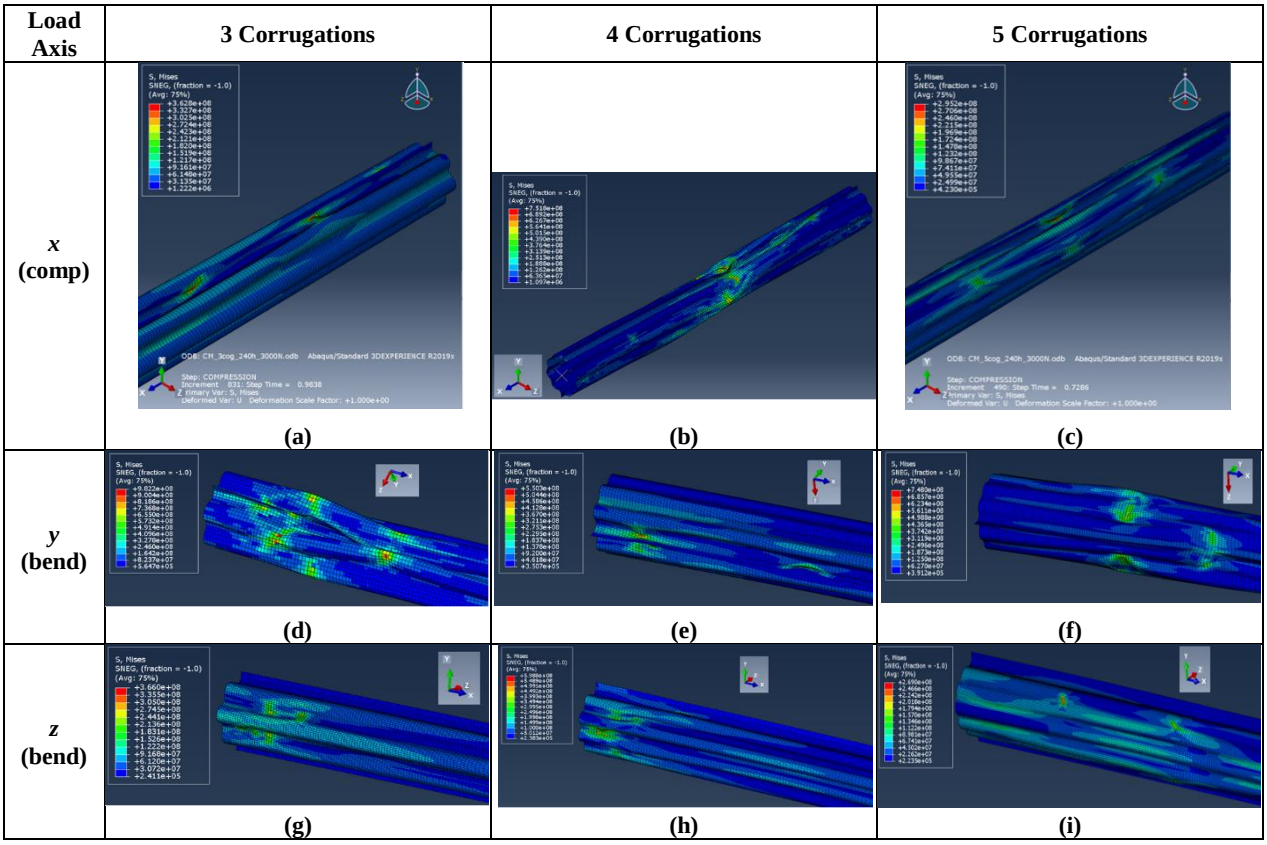

Fig. 11. Abaqus Von-Mises stress field and deformation shape at the reported critical buckling load under *y*-bending, *z*-bending and *x*-axial-compression for boom designs with different number of corrugations n = 3, 4, and 5.

Boom bending stiffness about the two principal axes y and z is proportional to the area moments of inertia about those axes, I_{yy} and I_{zz}. However, when evaluating the results of Fig. 9, one can see that even though the inertias grow with the number of corrugations, the bending strength is reduced. The boom design with n = 3 has a 6.2% and 45.2% improvement in y-axis bending strength with respect to the designs with n = 4 and n = 5 cases. The increase in z-axis bending strength for the boom design with n = 3 is 6.8% and 35.5%, respectively. At this boom size, bending strength quickly drops for corrugated designs with n > 4. A similar conclusion reached for the compression load cases can be adopted for the bending case. For a given boom size, as you grow the number of corrugations, the individual thin-shell segments of the boom become shallower and thus are more prone to local buckling when bending moments are applied to them. Therefore, a compromise between designing for bending stiffness and bending strength needs to be reached based on the needs of the structural application. For example, with the parameters chosen, if a balance between the two was sought after, a boom design with n = 4 might be adopted. If large bending strength with moderate stiffness is desired, a boom design with n = 3 would be adopted, and if large bending stiffness with moderate strength is desired, a boom design with n = 5 would be adopted.

Boom buckling loads and mode shapes can also be evaluated with a finite element eigenvalue buckling analysis. In Abaqus, using the previous finite element model described, a pre-load of 25 N for bending cases and 1000 N for compression was added using an initial nonlinear geometric static load analysis step before applying a unit load in the *BUCKLING step. In their short configuration analyzed, there are multiple buckling modes for these types of booms, making it difficult to find the mode which causes failure of the boom. The first 30 eigenfrequency buckling modes were requested in the simulation. Buckling modes and associated loads were matched with the critical loads predicted by the pure bending and compression simulations reflected in Fig. 10. Most buckling modes for each load case are similar to those displayed in Fig. 12. The bending simulations tend to fail in the bottom half of the boom, usually towards the boom root. For z-direction bending, booms almost always initially buckled locally at the concave

corrugations, as shown in Fig. 12 (a – c). Initial failure occurred in the web or web corrugation section r_w for y-direction bending, as shown in Fig. 12 (d – f). The compression simulations tended to present localized buckling in the center of the boom in the web corrugations and/or the web sections initially, as shown in Fig. 12 (g – i).

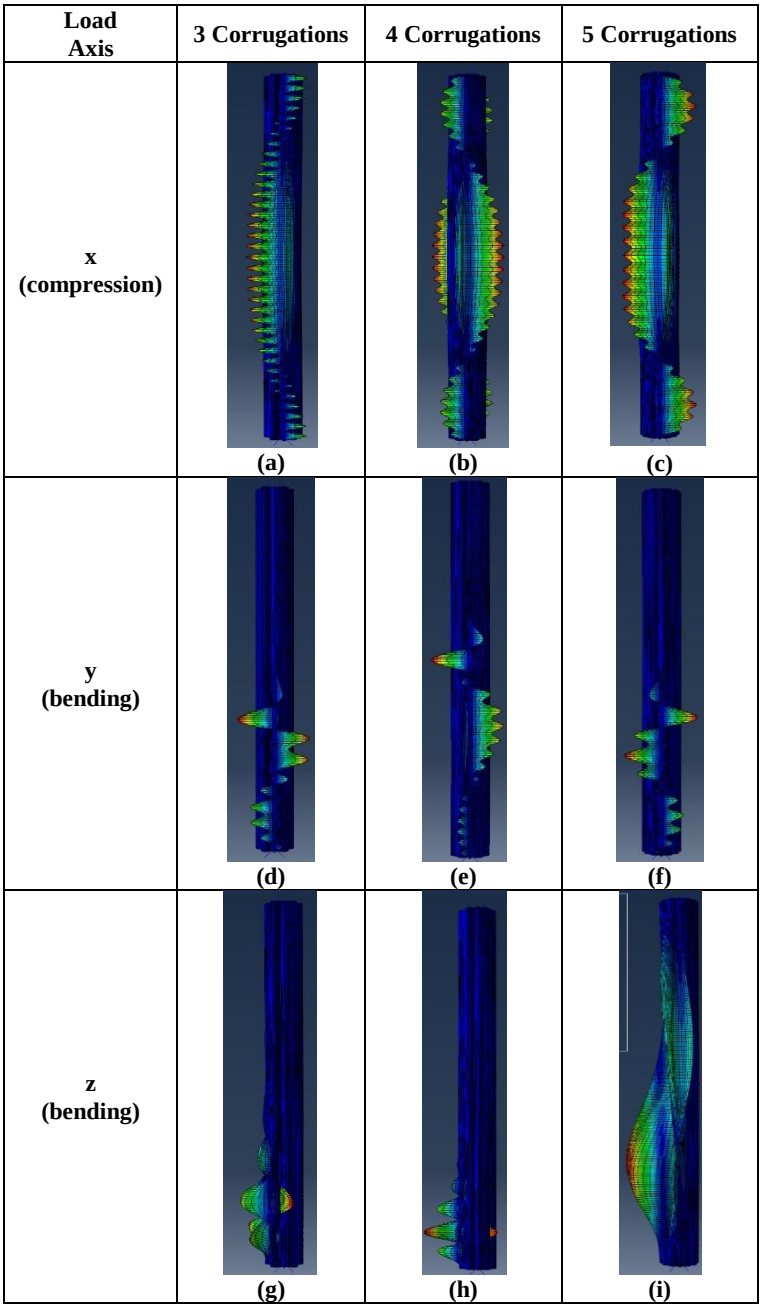

Fig. 12. Abaqus first buckling mode/shape predictions under y-bending, z-bending and x-axial-compression for boom designs with different number of corrugations n = 3, 4, and 5.

V. Sample Down-Select for Fabrication

From the parametric study results, six initial boom designs were selected for manufacturing based on their adequate structural properties and to investigate combinations of different geometric parameters. Dimensions of these booms are in Table 3 and are graphed in Fig. 12. Flattened heights of 130 mm, 190 mm, and 240 mm were selected. Two number of corrugations were selected for each flattened height. The smaller designs were chosen because they have the same flattened height as the largest CTM fabricated to date at LaRC and thus can be used as a one-to-one

comparison with that boom type. The remaining dimensions were selected to obtain relatively deep corrugations for each boom size for them to be meaningful and to maximize inertias. Note that the last boom design from Table 3 was analyzed in Section IV.

Six boom molds from the selected designs are being constructed from Last-a-foam® FR-4800 high-temperature tooling board from General Plastics. This new foam material offers a cost-effective alternative to other tooling methods with a low CTE similar to that of Aluminum and one-third of the density. The same scalable co-cured fabrication process developed for the large-scale CTM booms will be employed for manufacturing the proof-of-concept COROTUB specimens. This new method co-cures the two boom halves and bonds them in a single step, which simplifies the process, reduces fabrication costs, and produces relatively high-tolerance parts with low reject counts[26].

Table 3. Dimensions of Selected Booms to be Manufactured and Tested.

Size	h (mm)	n	w (mm)	r_w (mm)	r_v (mm)	r_c (mm)
Small	130	2	4.5	12	12	9
	130	3	4.5	12	9	9
Medium	190	3	9	12	12	9
	190	4	9	12	12	9
Large	240	3	9	12	16	12
	240	5	9	12	12	9

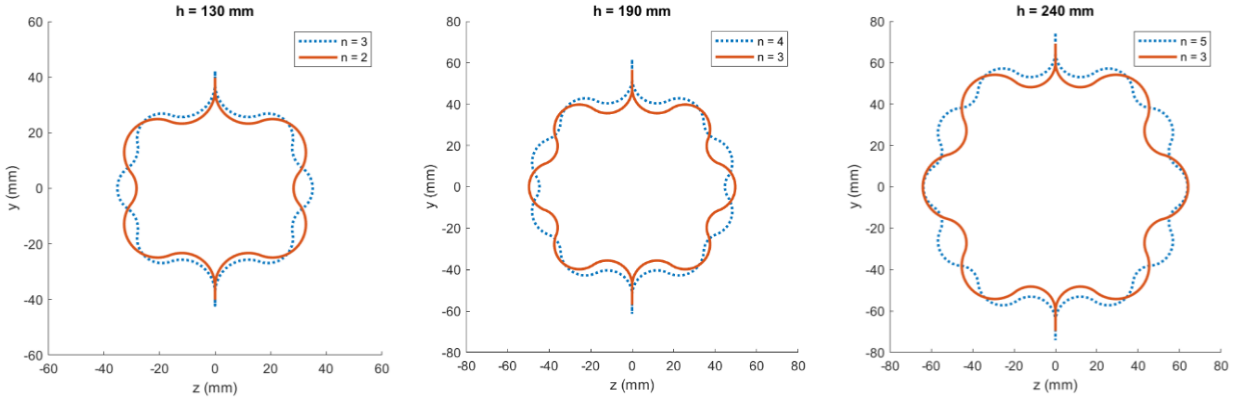

(a) (b) (c)

Fig. 12. Boom designs selected for fabrication, structural characterization and functional testing.

VI. Future Work

The additional work that will be presented in the final manuscript will include:

- Manufacturing and structural characterization of the deployed and coiled configurations of the six symmetric COROTUB designs selected by the parametric analysis. Boom specimens to be fabricated will be 1.22-m long. Molds are already under construction.
- Comparison of FEA versus experimental results for uniaxial load cases in axial compression and bending.
- Performance comparison with available CTM booms of the same size, i.e. h = 130 mm.
- Buckling FEA of preferred boom designs at 10 m and 16.5 m length scales.
- Conclusions that will drive the next steps of the design process towards optimizing the design of this new boom concept for increased structural properties.

References

[1]Fernandez, J. M. "Advanced Deployable Shell-Based Composite Booms for Small Satellite Applications including Solar Sails", *4th International Symposium on Solar Sailing*, Kyoto, Japan, 17-20 January 2017.

[2]Fernandez, J. M., et al., "An Advanced Composites-Based Solar Sail System for Interplanetary Small Satellite Missions", *5th AIAA Spacecraft Structures Conference, AIAA Scitech 2018 Forum*, Kissimmee, Florida, 8-12 January 2018.

[3]Rimrott, F.P.J., *Storable Tubular Extendible Member…A Unique Machine Element*, Machine Design, 37, No. 28, 156-165, 1965.

[4]Roybal, F.A., Banik, J.A., Murphey, T.W., *Development of an Elastically Deployable Boom for Tensioned Planar Structures*, 48th AIAA/ASME/ASCE/AHS/ASC Structures, Structural Dynamics and Materials Conference, Honolulu, Hawaii, April 2007.

[5]Francis, W. H., Freebury, G., Hulse, M. J., "Rigid Slit-Tube Laminate System", U.S. Patent 9,840,060, awarded on 12 December 2017.

[6]Daton-Lovett, A. J., "Coilable Extendible Member and Methods", U.S. Patent 10,100,951, awarded on 20 June 2017.

[7]Taylor, R., Turse, D., Adams, L. G., Reavis, M., Richardson, D., "Slit Tube Locking Longeron", U.S. Patent 10,544,900, awarded on 20 January 2020.

[8]Rehnmark, F., et al., "Development of a Deployable Nonmetallic Boom for Reconfigurable Systems of Small Spacecraft", *48th AIAA/ASME/ASCE/AHS/ASC Structures, Structural Dynamics, and Materials Conference*, Honolulu, Hawaii, 23-26 April 2007.

[9]Fernandez, J. M., "Sheath-Based Rollable Lenticular-Shaped and Low-Stiction Composite Boom", U.S. Patent 9,863,148, awarded 9 January 2018.

[10]Katsumata, N., Kaimori, M., Higuchi, K., Natori, M. C., Yamakawa, H., *Deployment Characteristics of Braided Coated Bi-Convex Tape and Bi-SMA Convex Tape Booms for Deployable Membrane Structures*, Journal of Mechanics Engineering and Automation, Vol. 4, pp. 52-62, 2014.

[11]Chubachi, T., Furuya, H., Watanabe, A., "Hybrid self-deployable Tubular CFRP Booms for Deployable Membrane", *4th International Symposium on Solar Sailing*, Kyoto, Japan, 17-20 January 2017.

[12]MacNaughton, J. D., et al., "The Bi-STEM – A new Technique in Unfurlable Structures" 2nd Aserospace Mechanism Symposium, Santa Clara, CA, pp. 139-145, 1967.

[13]Deployable Space Systems, URL: https://www.dss-space.com/products-boom-systems, accessed 5 June 2020.

[14]Rennie, B. B., "New Closed Tubular Extendible Boom", *2nd Aerospace Mechanisms Symposium*, ed: Herzl, G.G., JPL TM 33-355, pp.163-170, 1967.

[15]Crouch, D.S., *Mars Viking Surface Sampler Subsystem*, 25th Conference on Remote Systems Technology, 1977.

[16]Aguirre-Martinez, M. A., Bureo-Dacal, R., Del Campo, F., Fuentes, M., "The CTM family of Masts and the CTM Engineering Model", *3rd European Space Mechanisms & Tribology Symposium*, Madrid, Spain, 1987

[17]Geppert, U., Biering, B., Lura, F., Block, J., Straubel, M., Reinhard, R., "The 3-step DLR-ESA Gossamer Road to Solar Sailing", Advances in Space Research, Vol. 48, pp. 1695-1701, 2011.

[18]NASA Space Technology Mission Directorate, Game Changing Development Program, URL: http://gameon.nasa.gov/projects/deployable-composite-booms-dcb

[19]Fernandez, J. M., Lee, A. J., "Bistability in Collapsible Tubular Mast Booms", *AIAA Scitech 2019 Forum*, San Diego, California, 7-11 January 2019.

[20]Lee, A. J., Fernandez, J. M., "Inducing bistability in Collapsible Tubular Mast booms with thin-ply composite shells", Composite Structures Vol. 225, 111166, 2019.

[21]Fernandez, J. M., Krizan, S. A., Dyke, E. R. "Thin-Shell Deployable Composite Booms for Solar Sails: Design, Manufacturing, and Qualification", *5th International Symposium on Solar Sailing*, Aachen, Germany, 30 July- 2 August 2019.

[22]Okada, H., Furuya, H., "Concept and Structural Properties of Deployable Boom with Corrugated Closed Section", *69th International Astronomical Conference*, Bremen, Germany, 1-5 October 2018.

[23]Furuya, H., Okada, H., "Deployment and Retraction Demonstration of Corrugated Closed-Section CFRP Booms", *AIAA Scitech 2020 Forum*, Orlando, Florida, 6-10 January 2020.

[24]Johnson Jr, R., "Design and Fabrication of a Ring-Stiffened Graphite-Epoxy Corrugated Cylindrical Shell", NASA CR-3026, 1978.

[25]Ning, X., Pellegrino, S., "Imperfection-insensitive axially loaded thin cylindrical shells", International Journal of Solids and Structures Vol. 63, pp. 39-51, 2019.

[26]Fernandez, J. M., McLain, K. J., "Single-step co-cured manufacturing process of closed-section hollow composite structures with complex shapes", NASA Case No. LAR-19445-1, July 2019.